Proceedings of the ASME 2023
Conference on Smart Materials, Adaptive Structures, and Intelligent Systems
SMASIS2023
September 11-13, 2023, Austin, TX, USA

SMASIS2023-111012

SOFT ACTUATORS FROM FLEXIBLE AUXETIC METAMATERIALS AND SHAPE MEMORY ALLOYS SPRINGS

Janghoon Woo[1], Julianna Abel[1]

[1]Mechanical Engineering, University of Minnesota Twin Cities, Minneapolis, MN

ABSTRACT

Soft robots composed of elastic materials can exhibit nonlinear behaviors, such as variable stiffness and adaptable deformation, that are favorable to cooperation with humans. These characteristics enable soft robots to be used in multiple applications, ranging from minimally invasive surgery and search and rescue in emergency or hazardous environments to marine or space exploration and assistive devices for people with musculoskeletal disorders. Although soft actuators composed of smart materials have been proposed as a control strategy for soft robots, most studies have focused on traditional actuators using hydraulic or pneumatic pressure. Over the years, these have made a lot of progress, but they have not been able to overcome the limitations of the complex configuration of the system and the expansion of the cross-section of the actuator when contracted. This paper merges the actuator design methodology for smart materials with the mechanical analysis of auxetic structures to present an electrically driven soft actuator architecture that achieves reliable actuation displacements. This novel soft actuator, constructed with contractile SMA springs and flexible auxetic metamaterials (FAM), has a spontaneous recovery of the shape after a contraction, a negative Poisson's ratio, and over 90% of consistency with the performance predictions at the design stage. Our research presents a methodology for the design of a new electrically driven soft actuator, describes the manufacture of SMA springs and FAM, and concludes with the validation of the design by experimental analysis using the 2D planar soft actuator prototype. Finally, our study revealed that the application of the extraordinary characteristics of smart materials and structures together into a single architecture can be a strategy to overcome the limitations of existing soft actuator studies.

Keywords*: shape memory alloy, auxetics, soft actuator*

1. INTRODUCTION

Conventional robots developed for industrial applications are generally made of hard, rigid materials and show predictable linear motion. These robots can perform precise and rapid repetitive tasks that are difficult to implement by humans. However, due to the physical limitations of traditional robots [1], such as limited mobility and lack of adaptability restricting their ability to navigate complex environments or perform intricate tasks, many challenges in various industries remain difficult to solve and require a new robot paradigm.

Flexible materials and bioinspired design have enabled structurally reconfigurable soft robots characterized by adaptive, flexible interaction with unpredictable surroundings [2]. Unlike traditional rigid metal-based robot systems with multiple joints, soft robots designed with elastic materials can be simpler and cheaper to manufacture and exhibit nonlinear behavior favorable to cooperation with humans [3]. Soft robots have great potential for applications such as medical diagnostics and minimally invasive surgery [4], search and rescue in emergency or hazardous environments, marine or space exploration [5]–[11], and assistive devices for people with musculoskeletal disorders [12], [13].

To improve the operation of soft robots, control strategies that use traditional actuators (pneumatic, hydraulic, and motor-based systems) or smart material actuators (electroactive polymers, shape memory alloys, and polymers, and ferromagnetic elastomers) have been proposed and demonstrated [14], [15]. Despite the rapid increase in soft robot-related publications over the last decade, most research has focused on pneumatic or hydraulic actuation approaches.

Soft actuators or artificial muscles that rely on hydraulic or pneumatic systems are usually composed of a deformable chamber [16]. The global deformation of the actuator is induced by the change in volume or pressure of the inner chamber by the external input. Using the force applied to both ends of the actuator is the primary operating principle of most soft actuators. This bladder-based approach inevitably widens the cross-section

of the actuator while it deforms [17]. This characteristic is found in most studies of soft robots or grippers that mimic human hands.

This research presents a new structural approach that combines smart materials and auxetic structures to create soft actuator systems with novel kinematic performance. By merging the actuator design methodology for smart materials with the mechanical analysis of auxetic structures, we present an electrically driven soft actuator architecture that achieves reliable actuation displacements. In addition, we present a brief background on the behavior of shape memory alloy actuators and auxetic structures, followed by design criteria for soft actuators to lay the foundation for the new soft actuator systems. This study analyzes the thermo-mechanical behavior of SMA springs, defines the re-entrant auxetic unit cell, mechanically analyzes the flexible auxetic metamaterials (FAM), determines the geometry of SMA springs and FAM, and designs and manufactures a full-actuator. A final proof of concept prototype was validated by comparing the performance evaluation results according to electrical input control with the performance prediction results obtained in the design stage. This research revealed that the application of the extraordinary characteristics of smart materials and structures together into a single architecture can be a strategy to overcome the limitations of existing soft actuator studies.

2. MATERIALS AND STRUCTURES

It is necessary to develop soft actuators with reliable performance and easy and precise control for soft robotic functions such as nonlinear motion, variable stiffness, and adaptable contact. Toward this, we created a new actuator architecture with shape memory alloys (SMA) springs and flexible auxetic metamaterials (FAM). This section will describe the fundamental characteristics of the shape memory effect and auxetic structures, as well as the geometries, materials, and detailed manufacturing processes of SMA springs and FAM.

2.1 Shape Memory Alloys (SMA)

The mechanical (shape memory effect, superelasticity, and high damping capacity) and chemical (biocompatibility and corrosion resistance) properties of SMA have attracted considerable interest from researchers [18]. These multiple characteristics make them useful in various applications, including aerospace, medical devices, and robotics [19]. We apply the shape memory effect to develop a soft actuator that operates only with electrical input [20], [21]. In this section, the basic knowledge required to understand the characteristics of SMA springs and the detailed manufacturing process of SMA springs will be described.

2.1.1 Shape Memory Effect

In contrast to the stereotype of material properties, elasticity can be observed not only in rubber-like polymers but also in metals. Whether a metal will exhibit elastic behavior in response to an external force can be predicted based on the yield strength of the material. However, since metals have a very small elastic strain range, spontaneous restoration to their original shape is impossible when large deformation occurs. Because of this common limitation of metals, SMAs that have the ability to return to a pre-defined shape or configuration after deformation is unique. This fascinating phenomenon, known as the shape memory effect (SME), has led to the development of many innovative technologies and opened up new avenues for scientific research [22]. It arises due to a reversible solid-state transformation between the austenite and martensite phases, which is a rearrangement of the crystalline structure of the constituent materials. Figure 1 explains SME by showing how an SMA spring is deformed by a load and restored to its initial shape by subsequent heating and unloading and the crystalline structure of the SMA material corresponding to each case.

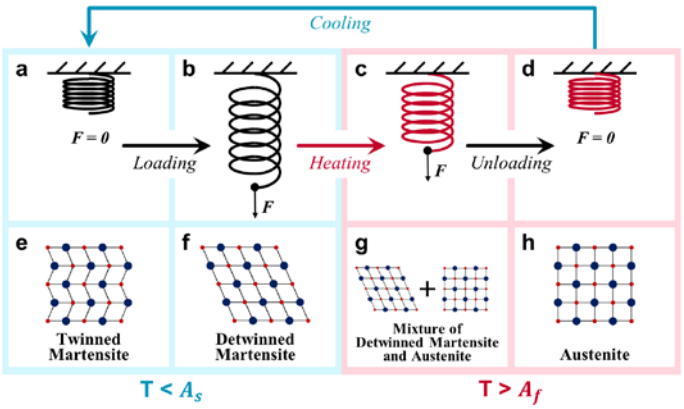

Figure 1: Shape memory effect. (a-d) Schematic diagrams representing the process in which an SMA spring is deformed by a load and restored to its initial shape by subsequent heating and unloading, and (e-h) the crystalline structure of the SMA material corresponding to each case. An initially (e) twinned martensite is deformed at a temperature lower than the austenite start temperature, making it (f) detwinned martensite. This leads to a change in macroscopic shape of SMA spring from (a) to (b). By heating above the austenite finish temperature, SMA spring's crystalline structure which was detwinned martensite turns into the (g) mixture of detwinned martensite and austenite. SMA spring recovers some deformation by heating, but remain deformed because there is still a load. When the load is removed from the SMA spring, it becomes (h) complete austenite and restores (d) its initial shape. Then, when the SMA spring is cooled below the austenite start temperature, its crystalline structure becomes twinned martensite again.

In SMA, the high-temperature phase is called austenite, while the low-temperature phase is called martensite. The austenite is the original crystal structure of the SMA, and it is characterized by a high degree of symmetry and a more uniform crystal structure than the martensite. There are two types of martensite: twinned martensite and detwinned martensite. Twinned martensite is characterized by the presence of twins, which are regions of the crystal lattice that are mirror images of each other. The twin structure results in a lower strain energy,

allowing the twinned martensite phase to be easily deformed [23]. When the SMA is deformed by the application of external stress, it undergoes a process known as reorientation, in which the martensite crystals begin to change orientation and align themselves in a more uniform manner. During this reorientation process, the twin boundaries in the martensite crystals become unstable and begin to break apart, resulting in the formation of more uniform detwinned martensite crystals. When the SMA is heated back above its transformation temperature, the crystals revert to their original austenite form. The temperature at which this transformation occurs depends on the specific alloy composition [24]. Once the SMA has transformed back into the austenitic phase, it can be deformed and then returned to its original shape, memorized in the material by the shape-setting process. This transformation is accompanied by a significant increase in the material's mechanical properties, such as stiffness and strength [19]. And this makes SMA useful in various applications, including actuators, biomedical implants, and compression garments for astronauts [25]–[29].

2.1.2 SMA Springs Fundamentals

A spring is a mechanical component that stores and releases energy through deformation. The geometry and composition of a spring play a critical role in determining its performance characteristics. The geometry of a spring is defined by its shape, size, and configuration. The composition of a spring refers to the materials used to manufacture it. The appropriate choice of geometry and material is critical to ensure that a spring performs its intended function effectively and efficiently.

The spring constant of a helical spring depends on its wire diameter and the mean diameter of a spring. Increasing the wire diameter or reducing the mean diameter will increase the spring constant. And in general, the spring constant determines its stiffness. The same trend is also seen in the SMA springs. In the case of the SMA spring composed of actuator wire, the larger the spring constant, the greater the contractile force for the same strain. Therefore, changing the geometry of an SMA spring can have a significant effect on its spring constant and its performance characteristics. This is important when designing an SMA spring for soft actuator applications, as the spring constant needs to be carefully selected to ensure that it performs as intended.

The SMA springs designed for the research all had the same inner diameter of 0.1835 inches. In addition, the distances between adjacent wires on the coil structure were all set to zero to maximize the contractile force of the SMA springs. Therefore the final spring pitch would be identical to the diameter of the SMA wire. As a result, the calculated spring constants for SMA springs manufactured from actuator wires having a wire diameter of 0.020 inches, 0.015 inches, and 0.012 inches are 10.175, 13.233, and 16.292, respectively (see Figure 2).

2.1.3 Manufacture of SMA Springs

The shape shape-setting process is a crucial step in the manufacture of SMA springs, where the alloy is programmed to remember a specific shape, is a crucial step in manufacturing

Inner diameter (inches)	0.1835		
Wire diameter, W.D. (inches)	0.020	0.015	0.012
Spring constant (= Mean diameter of a spring / W.D.)	10.175	13.233	16.292

Figure 2: Geometry of SMA springs. Schematic diagram of SMA springs of different geometries to be produced through the shape-setting process, and calculated spring constant results.

SMA springs. The procedures required for this process are as follows: 1) The SMA is mechanically deformed into the desired shape at room temperature while being held in a fixture. This was done by wrapping the SMA wire onto the connecting rod. 2) The deformed SMA is heated to a temperature above its transformation temperature, also known as the austenite finish temperature. This step was done in a furnace at 500℃. 3) The SMA is held at the elevated temperature for a period of time to allow it to transform into the austenite phase and relieve any internal stresses that may have been introduced during the pre-deformation step. Considering the composition and thickness of the SMA wire, the SMA wound on the fixture was heated for 5 minutes. 4) The SMA is then cooled down to room temperature while maintaining the desired shape. This step was done by putting the SMA in the water and to quenching it. 5) Finally, the fixture is removed, and the SMA will remember this shape and have a helical spring structure.

Figure 3a shows the SMA wire wrapped onto a stainless steel connecting rod with an outer diameter of 0.1835 inches. Nickel-titanium actuator wires (Flexinol®, Dynalloy, Inc.) with a rated austenite finish temperature ($A_{f,r} = 90℃$) were utilized to manufacture SMA springs responsible for actuation in the soft actuator. The coupling nuts, connecting rod, and serrated flange locknuts used for this process can be seen in Figure 3b-d. They all have a 10-32 thread. Given the temperature of 500℃ where the shape-setting process occurs, and the chemical stability required for the fixture, all parts made of 18-8 stainless steel were selected for use. Regardless of the thickness of the SMA wire, the same parts constituting the fixture were used. As a result, the SMA springs have the same inner diameter as shown in the schematic diagram in Figure 2.

After the shape-setting process, the color of the SMA wire that makes up the SMA springs changes from dark gray to glossy blue because of oxidation. When the SMA wire onto the fixture is heated to a high temperature, the surface of the material reacts with the oxygen in the air inside the furnace, forming a thin layer

of oxide on the surface of the material. This oxide layer changes the color of the material, making it more bluish than the original material. While it alters the appearance of the material, it does not affect the thermo-mechanical properties of SMA springs.

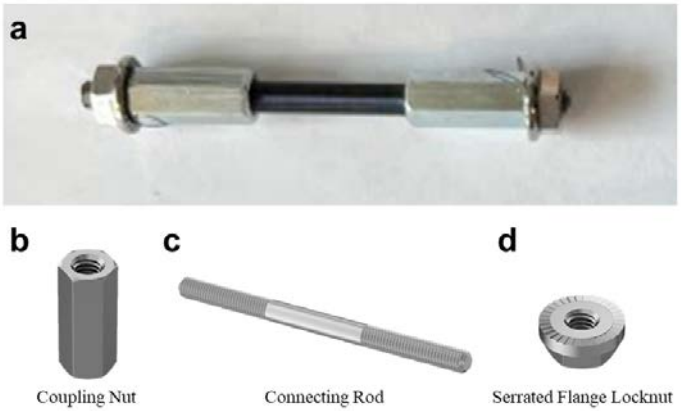

Figure 3: Preparation of the shape-setting process of SMA springs. (a) SMA wire firmly fixed in spring form on stainless steel parts, (b-d) Details of parts used as a fixture for shape-setting process.

2.2 Flexible Auxetic Metamaterials (FAM)

Auxetic structures or materials have a negative Poisson's ratio, meaning they expand in all directions when stretched rather than contracting like most materials [30]. Most auxetic structures have a void inside their geometry and are made of rigid materials. As a result, their manufacturing process is complex, which has made them of limited application in engineering. However, the advent of additive manufacturing technologies such as 3D printing has made manufacturing auxetics with different materials easier. And this has allowed auxetics to be used in many fields. In this section, we will briefly introduce the characteristics of auxetics, followed by a detailed description of the design and manufacturing process of the flexible auxetic metamaterials (FAM) that will serve as a bias spring in soft actuator architectures.

2.2.1 Types of Auxetic Structures

When a material is compressed in a particular direction, it is common for them to expand perpendicular to the applied stress. The property that characterizes the behavior of the material is Poisson's ratio. Most substances have a positive Poisson's ratio between 0.3 (glass) and 0.5 (rubber).

Auxetics are materials or structures that exhibit the unique property of negative Poisson's ratio, which means they contract in all directions when compressed instead of expanding in the transverse direction as in most materials (see Figure 4). The negative Poisson's ratio results in interesting mechanical properties such as vibration damping, energy absorption, enhancement of shear modulus, fracture toughness, and indentation resistance [31]–[33].

Despite the tremendous potential of these mechanical properties in many engineering fields, most auxetics are challenging to manufacture due to their complex geometries. Nevertheless, various auxetic materials and structures have been studied and reported. Initially, most studies were conducted on polymer foam structures, rotating squares, cubic metals, or cellular solids with a negative Poisson's ratio [34]–[36]. And recently, several other geometries have been studied, including re-entrant honeycomb, chiral, rotating polygonal, perforated, and folded geometries [37]–[41].

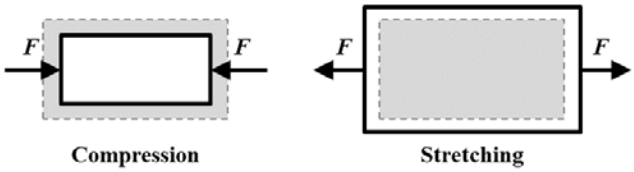

Figure 4: Behavior of auxetics. The dotted line represents the initial state of an arbitrary object. The schematic diagram on the left shows the state when the object is compressed by an external force, and the right side shows the state when it is stretched. As these two cases, when an arbitrary object has a negative Poisson's ratio, it can be referred to an auxetic structure or material.

2.2.2 Unit Cell Definition of FAM

The flexible auxetic metamaterial (FAM) that constitute the soft actuator can be formed by repeatedly arranging the re-entrant unit cell in a two-dimensional plane. The mechanical properties of the FAM can be adjusted through the changes in the geometry of the unit cell. This makes it possible to customize the performance of the FAM so that it is suitable for a particular application.

Re-entrant honeycomb geometry is a cellular structure consisting of hexagonal cells with an inner void connected to the adjacent cells by a smaller neck. When compressed, the honeycomb structure collapses in a specific sequence, causing the walls to buckle and the voids to contract, resulting in a negative Poisson's ratio.

The geometry and dimensions of the re-entrant unit cell used to design the FAM are illustrated in Figure 5. Four variables can determine this. The wall thickness ($\boldsymbol{T_w}$) of the re-entrant unit cell drawn in thin lines was set to 0.7 mm. This value was chosen to take into account the flexibility of the hinges as well as the overall structure. Horizontal wall length ($\boldsymbol{L_h}$), which determines the overall size of the unit cell, was set to 10 mm. The internal angle ($\boldsymbol{\theta}$) of the unit cell with the inward-point protrusions was set to 60°. And inclined wall length ($\boldsymbol{L_i}$) was set to 5 mm, an appropriate value for two adjacent hinges not to meet each other. As a result, the distance between the hinges at the center line allows the FAM made of this unit cell to have a negative Poisson's ratio.

2.2.3 Materials and Manufacture of FAM

The Fused Deposition Modeling (FDM) type 3D printer used in the manufacture of FAM has many advantages such as cost-effectiveness, the versatility of various material selections including PLA, ABS, and more, and easy-to-use.

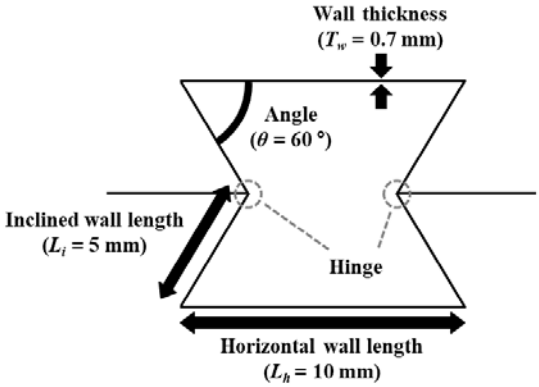

Figure 5: Geometry of re-entrant unit cell. The unit cell is determined by a total of four variables: Horizontal wall length (L_h), Inclined wall length (L_i), Wall thickness (T_w), and Angle (θ). At the center line of the unit cell, there are two adjacent hinges, which are indicated by gray dotted lines.

To print the FAM, a flexible 3D printer filament from NinjaTek (shore hardness of 85A) was used (see Figure 6a). It is made of Thermoplastic polyurethane (TPU) that does not wear or crack even after repeated elongation up to 660%. Figure 6b shows that a tabletop 3D printer (Lulzbot TAZ 6) utilizes this filament to print a FAM. A G-code that contains the instructions for the 3D printer to create each layer was prepared using the slicing software Cura-Lulzbot 3.6.25. The unit cell geometry (Figure 5) was printed to a depth of 10 mm.

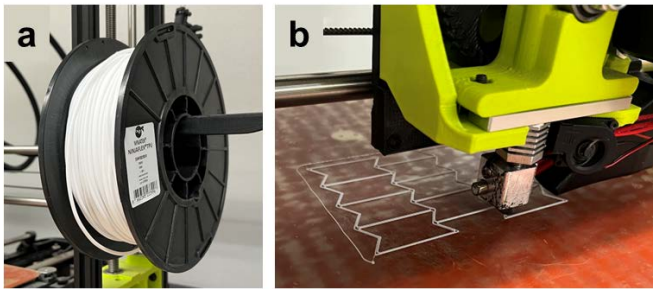

Figure 6: Materials and manufacture of FAM. (a) 3D printer filament made of Thermoplastic polyurethane (TPU), (b) Tabletop 3D printer printing a FAM.

3. SOFT ACTUATOR DESIGN

In the overall design and manufacturing process, soft actuators with flexible bodies differ from traditional actuators used in general machines or robots. In this section, the design criteria of the soft actuators, the proposed actuator architecture, and the experimental characterization results of the SMA springs and FAM will be described in detail.

3.1 Design Criteria of Soft Actuators

Soft actuators are useful for a variety of applications, including soft robotics, wearable devices, and biomedical devices. A good soft actuator has several characteristics that make it effective for its intended use [42]. In particular, it should be able to generate the required motion or force reliably while being flexible, durable, and scalable.

Soft actuators should be deformed easily without breaking or losing their ability to produce motion or force. This allows them to conform to different shapes and generate large displacements. In addition, they should be efficient in converting input energy into output force or motion. This means that they should be designed to minimize energy losses and maximize their ability to do work or make the desired motion. And they should be sufficiently durable to withstand repeated use without losing their original performance features. Lastly, they should be scalable, which means that they can be manufactured in different sizes and shapes to suit a variety of applications.

Design criteria for good soft actuators include: actuation mechanism, performance characteristics, material selection, geometry, manufacturing process, and environmental factors. It should be optimized to achieve the desired functionality in soft actuators. Soft actuators can be actuated by a variety of mechanisms. And the actuation mechanism should be selected based on the requirements of the application, such as displacement, output force, speed, or energy efficiency. The design should consider the required performance characteristics of the soft actuator. And these characteristics should be optimized to meet the specific requirements of the application. Soft actuators generally consist of parts made of flexible or deformable materials, such as elastomers, hydrogels, and shape memory polymers. And they often include components made of relatively stiff materials in their architecture. Therefore careful material selection should be made based on the actuation mechanism and required physical properties of the actuator. The geometry of the soft actuators plays a critical role in their performance. The design should consider factors such as shape, size, thickness, and the number of SMA required to achieve the desired motion or force. The manufacturing process of soft actuators should be scalable and repeatable. And the manufactured actuators should produce consistent and reliable performance. Lastly, appropriate materials and design should be selected to ensure the actuator can operate reliably in the intended environment. These considerations are all reflected in the soft actuator design that operates with a novel actuation mechanism proposed in this paper.

3.2 Soft Actuators Architecture

Systematically predicting the operational scenarios of the designed actuator is of great help in minimizing potential trial and error in subsequent processes. In this section, we propose an architecture of a soft actuator that works with a single input, and describe its operating principle. Based on an understanding of the physical characteristics and design constraints of the major primary two components of the soft actuator, the design strategy of the peripheral parts required to combine them into an integrated system will be outlined.

3.2.1 Combination of SMA Springs and FAM

A simple soft actuator design was suggested to build a soft actuator that is not dependent on pneumatic or hydraulic pressure systems. The composition and operating principle of the soft actuator and its shape before and after actuation are shown in Figure 7. SMA springs and FAM play the roles of contraction and biasing spring, respectively, which enables the soft actuator to produce repetitive actuation displacements. To obtain the large stroke length in the actuator, SMA was used in the form of a helical spring. And the flexibility and elasticity were achieved by incorporating the FAM made of flexible 3D printer filament into the soft actuator design.

Figure 7a shows the shape of the actuator when the SMA springs are heated and contracted. Here, it is assumed that the SMA springs are heated to a temperature higher than the austenite finish temperature of SMA. The deformation of the actuator to Figure 7b occurs when the SMA springs are cooled to room temperature. As a result, the actuator can restore its initial shape as shown in Figure 7b. No energy other than electrical input to create joule heating would be needed to create this reversible deformation in a soft actuator.

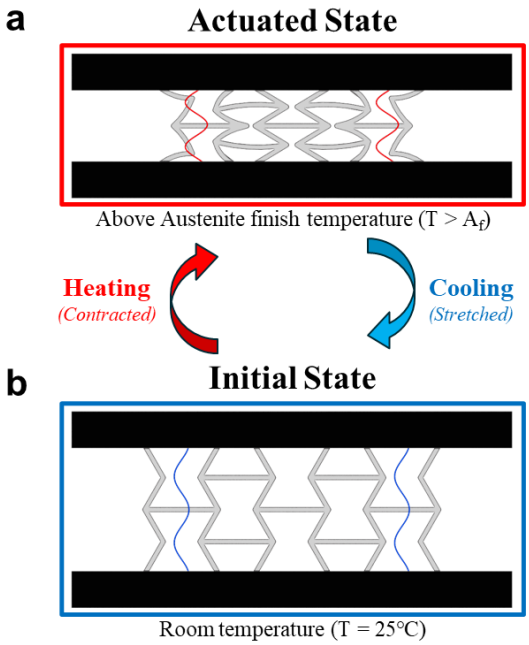

Figure 7: Schematic diagram of the soft actuator design with configuration and operating principle. SMA springs and FAM are combined to create the soft actuator. (a) SMA springs are contracted at the temperature above the austenite finish temperature $(\boldsymbol{T > A_F})$ and (b) elongated at room temperature $(\boldsymbol{T = 25}°C)$ to produce an actuation displacement of the soft actuator.

3.2.2 Consideration in the Design of Components Required to Assemble

Combining SMA springs, whose properties change rapidly with temperature change, and FAM with variable structural stiffness into an integrated system is as difficult as understanding the complex behavior of each. The scalability and energy efficiency of the soft actuator is greatly influenced by the connection parts of the two elements. Therefore, it is critical to understand the conditions required for 3D-printed parts and slip-free attachments for the SMA spring to be used in the actuator assembly process [43], and to design appropriate components that satisfy all of them.

3D printed parts manufactured using PLA were designed with the purpose of holding FAM and attachments for SMA spring firmly. 3D printed parts should have a small hole or gap where the wire connecting the attachments for SMA spring and the external power source can pass. And they should be designed in a form that minimizes the possibility of shape distortion due to a direct contact with the heated SMA. These considerations were applied to the design and fabrication process of the soft actuator prototype.

If the SMA spring slips even slightly during the actuation, it can cause significant errors in the soft actuator performance. The attachments that can firmly fix the SMA spring without slipping are designed as shown in Figure 8a. They will work by being located in pairs above and below the central SMA spring. The material constituting the attachments must be sufficiently thick and hard so that it does not tear or deform under the repeated actuation of the SMA spring. In addition, it is significant to properly design the cross-sectional shape of the attachments. They must include six or more small holes positioned symmetrically at a distance equal to the spring diameter of the SMA spring in the center of the structure. This can be seen in Figure 8b. These features of the attachments minimize the shape distortion of the connected SMA spring and enable the immediate transmission of the contractile force of the SMA spring to the FAM.

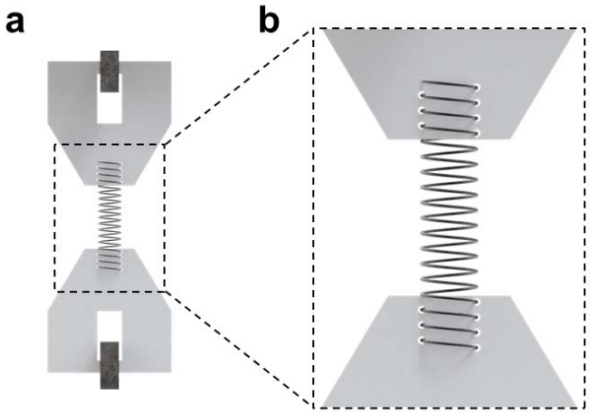

Figure 8: Schematic diagram of the slip-free attachments for SMA spring. (a) Arbitrary SMA spring fixed between two attachments, (b) An enlarged image of the location where the attachments and SMA spring are connected. The SMA wire passes along the small holes located in the attachments. The distance between two columns with holes is identical to the spring diameter of the SMA spring to minimize distortion in the shape of the SMA spring.

3.3 Thermo-mechanical Test of SMA Springs

In order to observe the contractile force and the change in stiffness while stretching the SMA spring, a solid coupling between the tensile test machine and the SMA spring must be guaranteed. In particular, since the characterization process of SMA spring is performed inside an environmental chamber with a temperature control function, this must be considered in the preparation of the experimental setup. This section will describe the details of the experimental setup and the results of the thermo-mechanical test of SMA springs.

3.3.1 Experimental setup for SMA Springs Characterization

The manufactured SMA springs were thermo-mechanically characterized by a uniaxial tensile test in a mechanical test machine with an environmental chamber attached. Slip-free attachments firmly holding the SMA spring and custom couples for the connection between the attachments and the pneumatic side-action grips were prepared for the characterization process.

In order to manufacture slip-free attachments, the water jet cutting was carried out using a 1mm thick aluminum metal plate. And then, eight holes were generated using a hand milling machine. Two custom couples for the connection between the slip-free attachments and the pneumatic side-action grips were manufactured using an aluminum block (see Figure 9a). The schematic on the left of Figure 9b shows how custom couples and slip-free attachments connect. Insulated high-temperature rubber tubing was placed at the location where the custom couples and the slip-free attachments meet to minimize the error caused by the shaking that may occur during the test. This is shown inside the ellipse drawn by the yellow dashed line on the right image of Figure 9b. The overall appearance of the experimental setup, in which the mechanical properties of the SMA spring are measured using the prepared parts, are shown in Figure 9c. And in this picture, an almost fully stretched SMA spring can be seen in the white dashed box. Figure 9d shows the initial state of the SMA spring. And the uniform deformation of the SMA spring and the firm fixation between the slip-free attachments and the SMA spring are shown in Figure 9e.

3.3.2 Characterization Analysis of SMA Springs

All displacement-control test was performed using a standard universal test machine of Instron (model #3365). The machine is equipped with a temperature-controlled environment chamber and pneumatic side-action grips (model #2732-009) capable of applying 60-70 psi pressure. Experiments were performed after immobilization of the sample in pneumatic side-action grips using custom couples and slip-free attachments. In order to characterize the SMA springs in the austenite and martensite phases, the tensile test was carried out in the environmental chamber temperature at 110°C and 25°C, respectively. During the test, the SMA springs were extended at a speed of 0.2 mm/s, and the resulting force was output in Newtons (N). Tensile deformation was applied to the SMA springs up to the limit of the point at which the relationship between applied force and structural strain maintained a linear relationship. The relationship

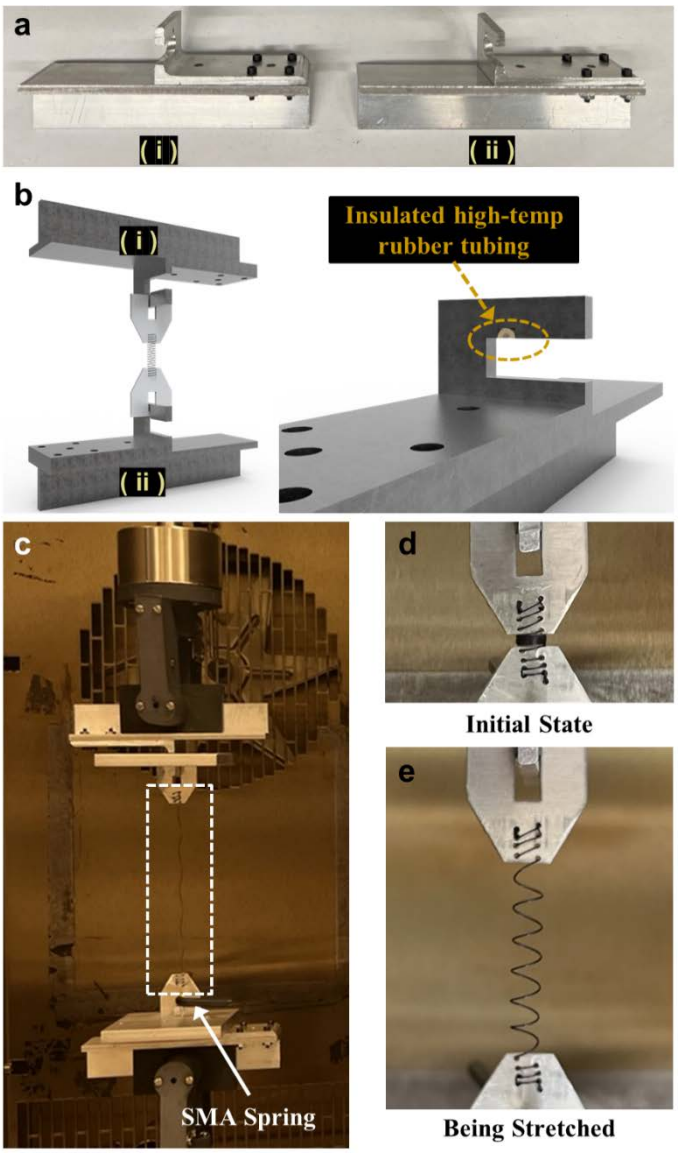

Figure 9: Experimental setup for SMA springs characterization. (a) Two custom couples (i, ii) made up of aluminum block for the connection between the slip-free attachments for SMA springs and the pneumatic side-action grips, (b) Schematic diagram and details of custom couple with insulated high-temperature rubber tubing, (c) Photo of SMA spring undergoing tensile test, Images of SMA spring in its (d) initial state and (e) being stretched.

between the applied force and the resulting strain of the material is typically described by Hooke's law, which states that the strain of an elastic material is directly proportional to the applied load. The proportional constant between the force and strain is a measure of the stiffness of the SMA spring.

The mechanical test results for three different SMA springs are shown in Figure 10. The color of the lines indicates the temperature condition above the austenite finish temperature (red) and at room temperature (blue). The structural strain of the

SMA spring is calculated based on the initial length of the SMA spring which was obtained by measuring the axial length of the spring structure when no load was applied to it. Although nearly similar displacements were applied in each experiment, each SMA spring had different maximum structural strain and stiffness. This is due to the difference in the thickness of the SMA wires used to manufacture the SMA springs, and the difference in the spring constant between each SMA spring. SMA springs with wire diameters of 0.015 inches and 0.020 inches exhibited stiffness values of approximately 4 and 10 times higher, respectively, compared to those with wire diameters of 0.012 inches. The mechanical properties of the SMA springs confirmed by this section are used as fundamental information to determine the geometry of the SMA springs and FAM constituting the soft actuator.

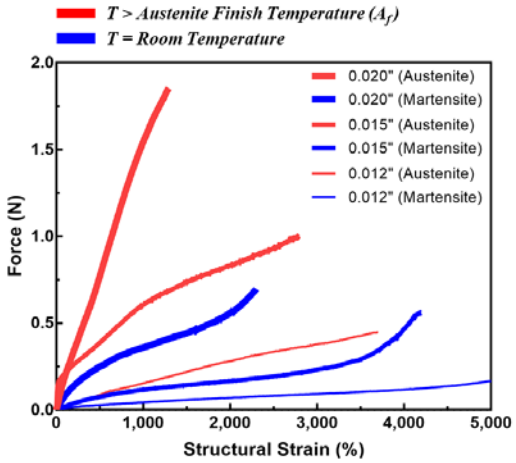

Figure 10: Uniaxial tensile test results for SMA springs with three different wire diameters. Red and blue color of the results indicate the temperature above the austenite finish temperature ($\boldsymbol{T > A_F}$) and at room temperature ($\boldsymbol{T = 25}$℃), respectively. Each results can be paired by the line thickness.

3.4 Mechanical Test of FAMs

The flexibility of FAM makes it difficult to predict how it deforms compared to general auxetic structures made of rigid materials. In addition, in order to confirm the characteristics of FAM having a two-dimensional planar shape, it is necessary to apply a load in the vertical direction as uniformly as possible. In this section, we will describe the details of the experimental set-up to minimize the instability caused by the FAM specimen bulged out to one side due to compression, the changes in the morphology and mechanical characterization results of FAM.

3.4.1 Experimental Setup for FAM Characterization

To facilitate accurate mechanical test of the FAM, sample holders to be coupled to the pneumatic side-action grip of the test machine were prepared. 3D-printed sample holders in black and purple can be seen in Figure 11a and Figure 11b. They were used to limit non-vertical movements, such as tilting or shifting to the left or the right in the FAM during the experiment. Consequently, the applied load only produces vertical displacement and motion in the FAM.

All experiments were performed at room temperature. The moving speed of the test machine jig was set to maintain a speed of 0.2 mm/s vertically downward direction. In addition, considering the measurement limit of the load cell used in the test, the experiment was set to terminate automatically at 50N.

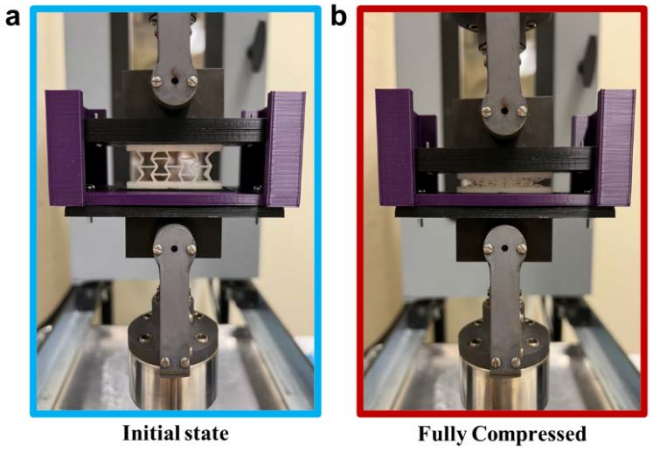

Figure 11: Experimental setup for FAM characterization. A photo of (a) the initial state of FAM located in the test machine and a photo (b) when it is fully compressed.

3.4.2 Changes in Morphology and Negative Poisson's Ratio

The front view of the uncompressed FAM can be seen through the upper left photo, highlighted by the light blue line, in Figure 12a. The height of the auxetic structure portion is shown under each image. It was measured by excluding the height of the upper and lower rectangular solid parts. All the images were taken while compressing the FAM by 1mm in the vertical direction until it was completely compressed. Its initial height is 16 mm, and when fully compressed, it becomes 5 mm. Then, as soon as the strain applied to the FAM disappeared, it returned to its original shape.

Unlike other auxetic structures made of rigid materials, the FAM shows bending not only in the hinges but also in the walls constituting the unit cell, mainly due to the flexibility of the material [44]. However, despite these differences, it does not affect the general trend of FAM having a negative Poisson's ratio.

Based on the movement of ten dots on the unit cell, colored by black and purple, the deformation of the unit cell was traced. In order to facilitate the comparison between each moment, the shapes of the unit cell were modelled. They were placed on the right side of Figure 12b-d. The Poisson's ratio of FAM can be calculated using the following equation,

$$\nu = -\frac{\Delta H/H}{\Delta W/W} \quad (1)$$

H and W refer to the height and width of the unit cell, respectively, and they can be seen on the right side of Figure 12b. When adjacent hinges at the center line of the unit cell are in contact and the unit cell is completely compressed, the calculated Poisson's ratios are -0.9354 and -1.6252, respectively (see Figure 12c and Figure 12d).

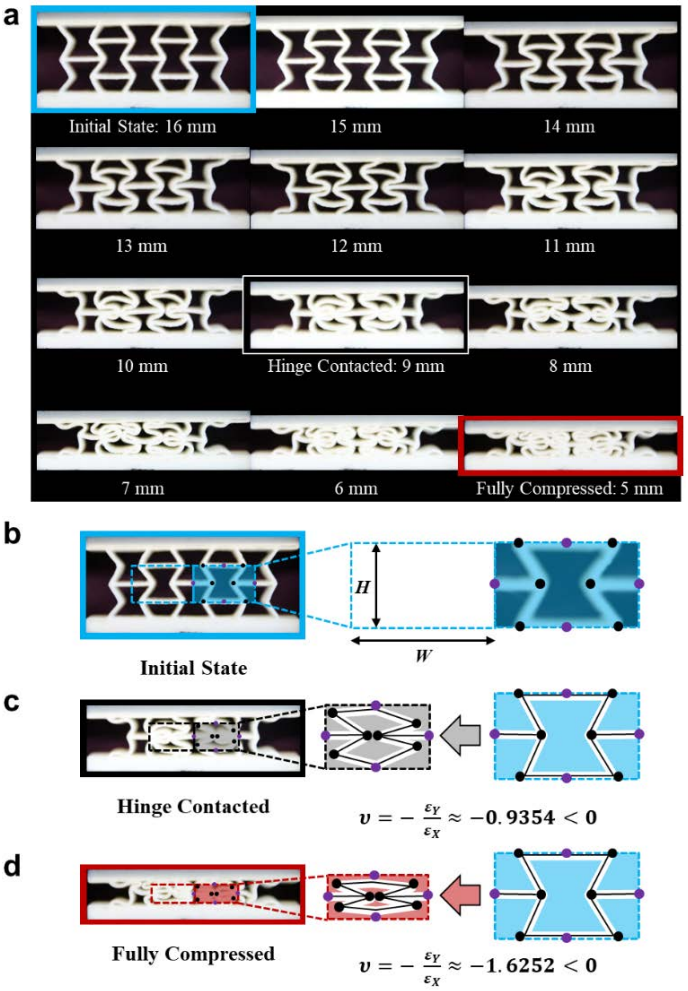

Figure 12: Morphology observation of FAM. (a) Photos of FAM taken with 1mm compressive deformation, (b) Photo of initial state of FAM unit cell used to calculate Poisson's ratio. H and W refer to the height and width of the unit cell, respectively. Poisson's ratio calculated based on the movement of ten dots, colored by black and purple, on the unit cell (c) when adjacent hinges on the centerline are in contact and (d) when the unit cell is completely compressed.

3.4.3 Characterization Analysis of FAM

As previously confirmed in the visual observation, the initial height of the uncompressed FAM used for characterization was also 16 mm. The experiment to measure the FAM's repulsive force against compressive load was terminated automatically when the measured force reached 50 N, as defined in the experimental setup step. Since the height of the FAM decreased during the experiment, the result in Figure 13 can be read from the bottom right to the left.

The result is consistent with the observation of changes in the morphology of FAM in Figure 12. The structural stiffness of the FAM increases rapidly when they are 9 mm and 5 mm in height. Images of the FAM corresponding to the initial state and the heights of 9 mm and 5 mm are shown on the respective height lines. The first increase occurs when the adjacent hinges at the center line come into contact with each other as compressive deformation progresses. The second increase occurs when the FAM is completely compressed, and finally, the inclined walls and the horizontal walls become almost parallel. Based on the results, the maximum displacement range of the FAM where it shows linear repulsive force was determined to be 7 mm, which is the displacement from the initial height of FAM to the point where adjacent hinges come into contact. We can conclude that this value depends on the geometry of the re-entrant unit cell constituting the FAM.

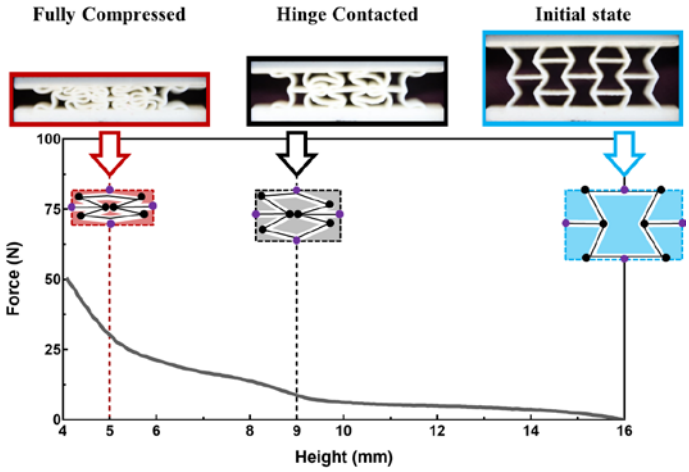

Figure 13: Characterization analysis of FAM. Changes in the repulsive force according to height and unit cell shape change due to compressive load in the vertical direction.

3.5 Determination Process of the Geometry of SMA Springs and FAM

In the process of designing a reliable soft actuator, it is important to determine which structures of SMA springs and FAM are to be used. Understanding the static equilibrium and a set of required performance and characteristics of the soft actuator leads to identifying the geometry of the main components that could generate the desired performance by a precise design process.

Except for the moment of actuation by contraction of the SMA springs, the soft actuator maintains a quasi-static equilibrium state. It is essential to identify all the loads and forces that can be applied to the actuator to design a soft actuator that meets specific requirements. The load and normal force applied to the components, as well as the forces exerted by SMA springs and FAM are illustrated in Figure 14a. Free-body diagrams on the left and right show the equilibrium of forces of the components when in the initial state and the actuated state,

respectively. The load can be divided into passive load and active load. Each corresponds to the load due to the weight of the components used to assemble the soft actuator and the tractive force necessary for the actuator. F_{load} refers to the sum of these two load. $F_{SMA,M}$ and $F_{SMA,A}$ refer to the contractile force exerted by the SMA spring in the martensite phase and the austenite phase, respectively. And $F_{Auxetics}$ refers to the repulsive force originating from FAM against compressive deformation.

Figure 14b, which can be obtained by overlapping the characterization results of SMA springs and FAM in one graph, enables the quantitative prediction of the performance of the designed soft actuator. In addition to the size of the active load, the stroke length which can be inferred from the location of the two intersections is also the important basis for the determination of the geometry of SMA springs and FAM. Based on these considerations, the process of designing an arbitrary soft actuator and evaluating its performance using a prototype will be described in the following chapter.

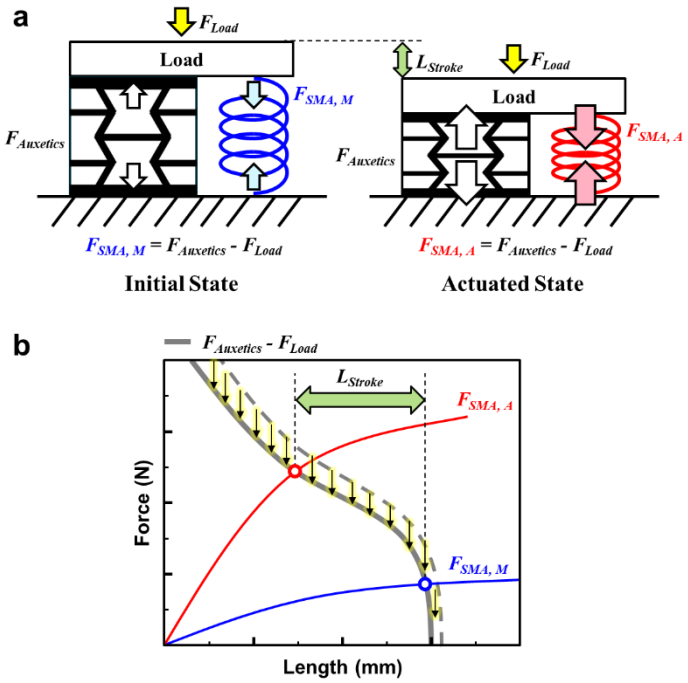

Figure 14: Determination process of the geometry of SMA springs and FAM. (a) Free-body diagram of the soft actuator in the initial state and the actuated state, (b) Performance prediction of the soft actuator through the comparison of characterization results of SMA springs and FAM.

4. SOFT ACTUATOR VALIDATION

Soft actuator architectures that operate only with electrical inputs are noteworthy in that few related technologies have been reported. However, in order to discuss its excellence and development potential, design assessment with prototypes should be preceded. In this section, we will estimate the performance of a soft actuator using the characterization results of SMA springs and FAM and assess the soft actuator design by comparing the prediction with the performance observed in the prototype. A step-by-step assembly plan of the prototype will be established considering the physical characteristics of the components and each function.

4.1 Behavior Prediction of Prototypes

For the design of the soft actuator prototype, component geometry determination strategies described in section 3.5 were used. Mechanical characterization results of the SMA springs and FAM confirmed in Figure 10 and Figure 13, respectively, were used as the basis for judgement in this process.

Among the SMA springs used in the uniaxial tensile test, the one made of the thickest wire exhibited the strongest force in the austenite phase for the same strain. With a wire diameter of 0.02 inches, it exerted a contractive force of about 1.5 N at 1000 % structural strain.

On the other hand, FAM, which applies force in the opposite direction to the SMA spring in soft actuator architecture, showed a rapid increase in force from a compressive displacement of about 7 mm. The force exerted by the FAM at this moment was about 8 N. Considering the difference in the magnitude level of forces originated from the SMA springs and the FAM, it was concluded that four SMA springs with the thickest wire diameter of 0.020 inches and one FAM should be used for the fabrication of the soft actuator prototype.

Figure 15a was obtained by superimposing the tensile test results of SMA spring with wire diameters of 0.020 inches (Figure 10) and the test results of FAM (Figure 13) on a single graph. Figure 15b was extracted to observe the part in Figure 15a where the length of the SMA spring and the height of the FAM had values between 10 and 16 mm. The points where the lines intersect in the graph and the point corresponding to the initial height of the FAM are numbered from i to v. Intersections are the points where the length, height, and force of the SMA spring and FAM coincide. Based on the location of these points, it was predicted that the length of the SMA spring would change as shown in Figure 15c according to the repeated heating and cooling cycles. The loop consisting of a dashed line highlighted in orange in Figure 15b and Figure 15c refers to the repeated actuation cycles according to the temperature control. L_{A_f} is the minimum length of the SMA spring at a temperature higher than the austenite finish temperature, and L_M is the length that SMA springs will have when they are in the martensite phase. They are approximately 10.5 mm and 15.5 mm, respectively. As a result, the actuation stroke length of the soft actuator prototype, $L_M - L_{A_f}$, was predicted to be about 5 mm.

4.2 Manufacture of Prototypes

Based on the behavior prediction, a soft actuator prototype consisting of four SMA springs and one FAM was designed. This can be seen in the schematic diagram in Figure 16a. In order to obtain a uniform deformation in the prototype, the SMA

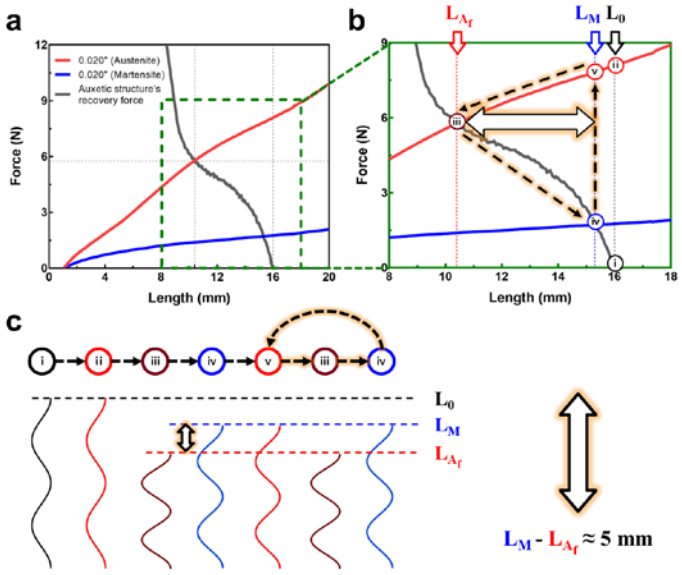

Figure 15: Behavior prediction of the soft actuator prototype. (a) Superimpose of the mechanical characterization results of the SMA spring and FAM and (b) its enlarged view, (c) A model that visualizes the length of the SMA spring at each point shown in (b). Actuation stroke length of the prototype was predicted to be about 5 mm.

springs must be located parallel to the central FAM and positioned symmetrically to each other. In addition to the SMA springs and FAM, attachments for SMA springs and 3D printed parts used in the assembly are also illustrated in Figure 16a.

Figure 16b shows in detail the assembly process for the complete soft actuator prototype in four steps as follows: i) Prepare the FAM to be located in the center of the soft actuator prototype. For the purpose of a firm and unshakable connection between the FAM and the bottom 3D printed parts, the FAM is designed with protruding parts at the top and bottom of its structure. ii) Fix all SMA springs between prepared attachments and ensure that they all have the same effective length. Each is then slowly deformed so that they all have a length that is the same height as the FAM. The effective length of the SMA springs after the extension is equal to L_0 shown in Figure 15b. iii) Attachments for SMA springs are fixed by 3D printed parts with rectangular shape protruding structures, acting as a rivet. iv) Finally, the 3D printed parts are combined in the upper parts of the FAM to complete the assembly of the soft actuator prototype.

4.3 Performance Evaluation

The actuation of the prototype was carried out by the joule heating of the SMA springs using the DC power. Cooling of the SMA springs was achieved by simply turning off the power input. The prototype, which was vertically compressed by the contraction of SMA springs, rapidly restored its original shape. One actuation cycle of the prototype took about 15 seconds.

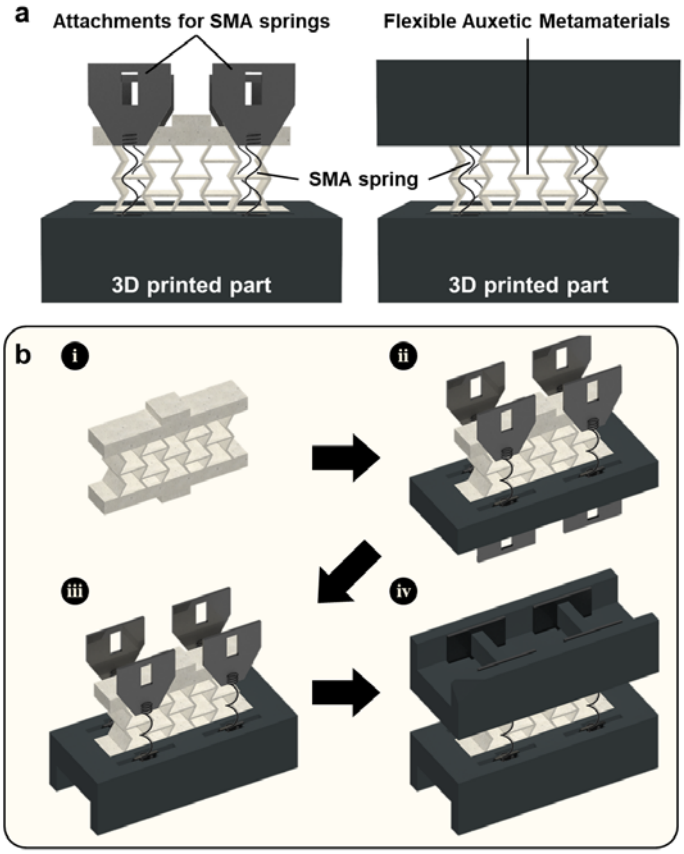

Figure 16: Fabrication process of the soft actuator prototype. (a) Schematic diagram of the soft actuator prototype and its composition, (b) Step-by-step assembly process of soft actuator prototype.

Figure 17a shows the results obtained by taking pictures of the manufactured prototype before and after actuation. Both the top and bottom images shown in Figure 17a were taken from the front of the soft actuator prototype. The arrows on the image represent the length and height of the SMA springs and FAM, respectively. And the observed actuator stroke length of the prototype was 4.5 mm. Figure 17b was created by modifying Figure 15b to facilitate a comparison between the behavior prediction in the design stage and the performance evaluation results of the prototype. The behavioral estimates had errors of less than 10% from the observed performance of the individual components, demonstrating the feasibility and potential of the proposed soft actuator design. This error can be improved by perfectly matching the lengths of the four SMA springs constituting the soft actuator and simultaneously contracting the SMA springs by applying electrical inputs in parallel. In addition, we observed 20 repetitive actuation cycles using the prototype and did not observe any performance degradation. Since the TPU constituting the FAM has excellent elastic properties, the performance of the soft actuator that generates fully reversible linear motion is expected to remain unchanged unless degradation occurs in the SMA springs.

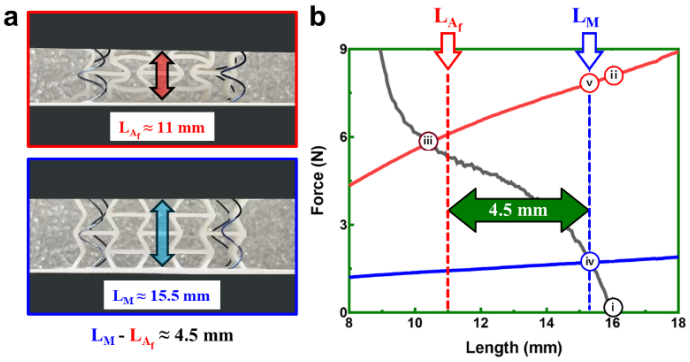

Figure 17: Performance evaluation of the soft actuator prototype. (a) Optical images of the soft actuator prototype before and after actuation. The observed actuator stroke length was approximately 4.5 mm. (b) Observed performance of the soft actuator prototype.

5. CONCLUSION

This paper presents a methodology for the design of a new electrically driven soft actuator, constructed with contractile SMA springs and FAM, has a spontaneous recovery of the shape after a contraction, a negative Poisson's ratio, and over 90% of consistency with the performance predictions at the design stage. In addition, this paper describes the manufacture of SMA springs and FAM, followed by the experimental validation of the design using a 2D planar soft actuator prototype. The SMA, which is responsible for the actuation of the soft actuator, was shape-set in the form of a spring for a large stroke length, and the FAM, which plays the role of an elastic bias spring in the actuator architecture, was produced by 3D printing using flexible TPU. Six criteria to be considered in designing a soft actuator operating with the proposed actuation mechanism were established based on the conditions required for a good actuator. A strategy to determine the geometry of the elements constituting a soft actuator that satisfies arbitrary requirements was suggested using the mechanical characterization results of SMA springs and FAM. The presented results validate the proposed design of a novel soft actuator using 2D planar soft actuator prototype fabricated as a proof of concept. The observed performance of the prototype showed a high agreement rate of over 90% compared to the prediction made at the design stage.

A soft actuator, composed of shape memory alloys and flexible auxetic structures, and does not depend on pneumatic or hydraulic systems, was designed, manufactured, and experimentally validated. The predictable and reliable performance of the prototype produced as a proof of concept suggests that the proposed actuation mechanism will be applied to the design of soft robot applications. The established design process can be implanted with other actuators, including SMA helical and overt-twisted coiled yarns. Future implementations of this actuation mechanism which can achieve the desired operation with only electrical energy, will dramatically simplify the overall design and manufacture of soft robot systems. In addition, the proposed actuation mechanism will be applied in the design of a system requiring a wireless control function. Through the design of an electrically driven soft actuator, this research addresses the challenges of achieving a reliable soft actuator design that does not depend on pneumatic or hydraulic pressure by establishing new actuation mechanisms with smart materials and auxetic structures.

ACKNOWLEDGEMENTS

This work was supported by an NSF CAREER Award Grant #1943715. We thank the Wearable Technology Laboratory at the University of Minnesota for the use of their Instron machine for the mechanical experiments.

REFERENCES

[1] J. Fryman and B. Matthias, "Safety of Industrial Robots: From Conventional to Collaborative Applications," presented at the ROBOTIK 2012; 7th German Conference on Robotics, VDE, May 2012.

[2] F. Iida and C. Laschi, "Soft Robotics: Challenges and Perspectives," *Procedia Comput. Sci.*, vol. 7, pp. 99–102, 2011, doi: 10.1016/j.procs.2011.12.030.

[3] D. Rus and M. T. Tolley, "Design, fabrication and control of soft robots," *Nature*, vol. 521, no. 7553, pp. 467–475, May 2015, doi: 10.1038/nature14543.

[4] H. Abidi *et al.*, "Highly dexterous 2-module soft robot for intra-organ navigation in minimally invasive surgery," *Int. J. Med. Robot.*, vol. 14, no. 1, p. e1875, 2018, doi: 10.1002/rcs.1875.

[5] M. A. Robertson and J. Paik, "New soft robots really suck: Vacuum-powered systems empower diverse capabilities," *Sci. Robot.*, vol. 2, no. 9, p. eaan6357, Aug. 2017, doi: 10.1126/scirobotics.aan6357.

[6] J. Byun *et al.*, "Underwater maneuvering of robotic sheets through buoyancy-mediated active flutter," *Sci. Robot.*, vol. 6, no. 53, p. eabe0637, Apr. 2021, doi: 10.1126/scirobotics.abe0637.

[7] S. Furukawa, S. Wakimoto, T. Kanda, and H. Hagihara, "A Soft Master-Slave Robot Mimicking Octopus Arm Structure Using Thin Artificial Muscles and Wire Encoders," *Actuators*, vol. 8, no. 2, p. 40, May 2019, doi: 10.3390/act8020040.

[8] T. Paschal, M. A. Bell, J. Sperry, S. Sieniewicz, R. J. Wood, and J. C. Weaver, "Design, Fabrication, and Characterization of an Untethered Amphibious Sea Urchin-Inspired Robot," *IEEE Robot. Autom. Lett.*, vol. 4, no. 4, pp. 3348–3354, Oct. 2019, doi: 10.1109/LRA.2019.2926683.

[9] Kenji Urai, Risa Sawada, Natsuki Hiasa, Masashi Yokota, and Fabio DallaLibera, "Design and control of a ray-mimicking soft robot based on morphological features for adaptive deformation," *Artif. Life Robot.*, vol. 20, no. 3, pp. 237–243, 2015, doi: 10.1007/s10015-015-0216-y.

[10] S.-J. Park *et al.*, "Phototactic guidance of a tissue-engineered soft-robotic ray," *Science*, vol. 353, no. 6295, pp. 158–162, Jul. 2016, doi: 10.1126/science.aaf4292.

[11] D.-Y. Lee, J.-K. Kim, C.-Y. Sohn, J.-M. Heo, and K.-J. Cho, "High–load capacity origami transformable wheel," *Sci. Robot.*, vol. 6, no. 53, Apr. 2021, doi: 10.1126/scirobotics.abe0201.

[12] P. Polygerinos, Z. Wang, K. C. Galloway, R. J. Wood, and C. J. Walsh, "Soft robotic glove for combined assistance and at-home rehabilitation," *Robot. Auton. Syst.*, vol. 73, pp. 135–143, Nov. 2015, doi: 10.1016/j.robot.2014.08.014.

[13] A. Ali, V. Fontanari, W. Schmoelz, and S. K. Agrawal, "Systematic Review of Back-Support Exoskeletons and Soft Robotic Suits," *Front. Bioeng. Biotechnol.*, vol. 9, p. 765257, Nov. 2021, doi: 10.3389/fbioe.2021.765257.

[14] J. Kim, J. W. Kim, H. C. Kim, L. Zhai, H.-U. Ko, and R. M. Muthoka, "Review of Soft Actuator Materials," *Int. J. Precis. Eng. Manuf.*, vol. 20, no. 12, pp. 2221–2241, Dec. 2019, doi: 10.1007/s12541-019-00255-1.

[15] I. Apsite, S. Salehi, and L. Ionov, "Materials for Smart Soft Actuator Systems," *Chem. Rev.*, vol. 122, no. 1, pp. 1349–1415, Jan. 2022, doi: 10.1021/acs.chemrev.1c00453.

[16] Charbel Tawk and Gursel Alici, "A Review of 3D-Printable Soft Pneumatic Actuators and Sensors: Research Challenges and Opportunities," *Adv. Intell. Syst.*, vol. 3, no. 6, pp. 2000223–2000240, Jun. 2021, doi: 10.1002/aisy.202000223.

[17] M. S. Xavier, A. J. Fleming, and Y. K. Yong, "Finite Element Modeling of Soft Fluidic Actuators: Overview and Recent Developments," *Adv. Intell. Syst.*, vol. 3, no. 2, p. 2000187, Feb. 2021, doi: 10.1002/aisy.202000187.

[18] A. D. Johnson, V. Martynov, and V. Gupta, "Applications of shape memory alloys: advantages, disadvantages, and limitations," presented at the Micromachining and Microfabrication, J. M. Karam and J. A. Yasaitis, Eds., San Francisco, CA, Sep. 2001, pp. 341–351. doi: 10.1117/12.442964.

[19] Leonardo Lecce and Antonio Concilio, *Shape memory alloy engineering: for aerospace, structural and biomedical applications*. Elsevier, 2014.

[20] J. Mohd Jani, M. Leary, and A. Subic, "Designing shape memory alloy linear actuators: A review," *J. Intell. Mater. Syst. Struct.*, vol. 28, no. 13, pp. 1699–1718, Aug. 2017, doi: 10.1177/1045389X16679296.

[21] H. Rodrigue, W. Wang, M.-W. Han, T. J. Y. Kim, and S.-H. Ahn, "An Overview of Shape Memory Alloy-Coupled Actuators and Robots," *Soft Robot.*, vol. 4, no. 1, pp. 3–15, Mar. 2017, doi: 10.1089/soro.2016.0008.

[22] K. Otsuka and X. Ren, "Physical metallurgy of Ti–Ni-based shape memory alloys," *Prog. Mater. Sci.*, vol. 50, no. 5, pp. 511–678, Jul. 2005, doi: 10.1016/j.pmatsci.2004.10.001.

[23] G. B. Olson and M. Cohen, "Stress-assisted isothermal martensitic transformation: Application to TRIP steels," *Metall. Trans. A*, vol. 13, no. 11, pp. 1907–1914, Nov. 1982, doi: 10.1007/BF02645934.

[24] J. Frenzel, E. P. George, A. Dlouhy, Ch. Somsen, M. F.-X. Wagner, and G. Eggeler, "Influence of Ni on martensitic phase transformations in NiTi shape memory alloys," *Acta Mater.*, vol. 58, no. 9, pp. 3444–3458, May 2010, doi: 10.1016/j.actamat.2010.02.019.

[25] D. J. Fernandes, R. V. Peres, A. M. Mendes, and C. N. Elias, "Understanding the Shape-Memory Alloys Used in Orthodontics," *ISRN Dent.*, vol. 2011, pp. 1–6, Oct. 2011, doi: 10.5402/2011/132408.

[26] H. Holman, M. N. Kavarana, and T. K. Rajab, "Smart materials in cardiovascular implants: Shape memory alloys and shape memory polymers," *Artif. Organs*, vol. 45, no. 5, pp. 454–463, May 2021, doi: 10.1111/aor.13851.

[27] H.-T. Lee *et al.*, "Shape memory alloy (SMA)-based head and neck immobilizer for radiotherapy," *J. Comput. Des. Eng.*, vol. 2, no. 3, pp. 176–182, Jul. 2015, doi: 10.1016/j.jcde.2015.03.004.

[28] L. Petrini and F. Migliavacca, "Biomedical Applications of Shape Memory Alloys," *J. Metall.*, vol. 2011, pp. 1–15, May 2011, doi: 10.1155/2011/501483.

[29] K. Eschen, R. Granberry, B. Holschuh, and J. Abel, "Amplifying and Leveraging Generated Force Upon Heating and Cooling in SMA Knitted Actuators," *ACS Appl. Mater. Interfaces*, vol. 12, no. 48, pp. 54155–54167, Dec. 2020, doi: 10.1021/acsami.0c14206.

[30] R. Lakes, "Advances in negative Poisson's ratio materials," *Adv. Mater.*, vol. 5, no. 4, pp. 293–296, Apr. 1993, doi: 10.1002/adma.19930050416.

[31] Y. Liu and H. Hu, "A review on auxetic structures and polymeric materials," *Sci Res Essays*, vol. 5, no. 10, pp. 1052–1063, 2010.

[32] Y. Ma, F. Scarpa, D. Zhang, B. Zhu, L. Chen, and J. Hong, "A nonlinear auxetic structural vibration damper with metal rubber particles," *Smart Mater. Struct.*, vol. 22, no. 8, p. 084012, Aug. 2013, doi: 10.1088/0964-1726/22/8/084012.

[33] S. Bronder *et al.*, "Hybrid Auxetic Structures: Structural Optimization and Mechanical Characterization," *Adv. Eng. Mater.*, vol. 23, no. 5, p. 2001393, May 2021, doi: 10.1002/adem.202001393.

[34] R. Lakes, "Foam Structures with a Negative Poisson's Ratio," *Science*, vol. 235, no. 4792, pp. 1038–1040, Feb. 1987, doi: 10.1126/science.235.4792.1038.

[35] J. N. Grima and K. E. Evans, "Auxetic behavior from rotating squares," *J. Mater. Sci. Lett.*, vol. 19, pp. 1563–1565.

[36] R. H. Baughman, J. M. Shacklette, A. A. Zakhidov, and S. Stafström, "Negative Poisson's ratios as a common feature of cubic metals," *Nature*, vol. 392, no. 6674, pp. 362–365, Mar. 1998, doi: 10.1038/32842.

[37] K. W. Wojciechowski, "Two-dimensional isotropic system with a negative poisson ratio," *Phys. Lett. A*, vol. 137, no. 1–2, pp. 60–64, May 1989, doi: 10.1016/0375-9601(89)90971-7.

[38] V. V. Novikov and K. W. Wojciechowski, "Negative Poisson coefficient of fractal structures," *Phys. Solid State*, vol. 41, no. 12, pp. 1970–1975, Dec. 1999, doi: 10.1134/1.1131137.

[39] B. Chambers, F. Scarpa, and F. C. Smith, "The electromagnetic properties of re-entrant dielectric

honeycombs," *IEEE Microw. Guid. Wave Lett.*, vol. 10, no. 11, pp. 451–453, Nov. 2000, doi: 10.1109/75.888829.
[40] K. W. Wojciechowski, "Non-chiral, molecular model of negative Poisson ratio in two dimensions," *J. Phys. Math. Gen.*, vol. 36, no. 47, pp. 11765–11778, Nov. 2003, doi: 10.1088/0305-4470/36/47/005.
[41] Wm. G. Hoover and C. G. Hoover, "Searching for auxetics with DYNA3D and ParaDyn," *Phys. Status Solidi B*, vol. 242, no. 3, pp. 585–594, Mar. 2005, doi: 10.1002/pssb.200460377.
[42] P. Boyraz, G. Runge, and A. Raatz, "An Overview of Novel Actuators for Soft Robotics," *Actuators*, vol. 7, no. 3, p. 48, Aug. 2018, doi: 10.3390/act7030048.
[43] S. Enemark, I. F. Santos, and M. A. Savi, "Modelling, characterisation and uncertainties of stabilised pseudoelastic shape memory alloy helical springs," *J. Intell. Mater. Syst. Struct.*, vol. 27, no. 20, pp. 2721–2743, Dec. 2016, doi: 10.1177/1045389X16635845.
[44] Y. Jiang and Y. Li, "3D Printed Auxetic Mechanical Metamaterial with Chiral Cells and Re-entrant Cores," *Sci. Rep.*, vol. 8, no. 1, p. 2397, Dec. 2018, doi: 10.1038/s41598-018-20795-2.